A Quantitative Analysis of Light-Driven Charge Transfer Processes Using Voronoi Partitioning of Time Dependent DFT-Derived Electron Densities

Jeroen A. Rombouts,[a] Andreas W. Ehlers,*[a,b] and Koop Lammertsma *[a,b]

An analytical method is presented that provides quantitative insight into light-driven electron density rearrangement using the output of standard time-dependent density functional theory (TD-DFT) computations on molecular compounds. Using final and initial electron densities for photochemical processes, the subtraction of summed electron density in each atomcentered Voronoi polyhedron yields the electronic charge difference, Q^{VECD}. This subtractive method can also be used with Bader, Mulliken and Hirshfeld charges. A validation study shows Q^{VECD} to have the most consistent performance across basis sets and good conservation of charge between electronic states. Besides vertical transitions, relaxation processes can be investigated as well. Significant electron transfer is computed for isomerization on the excited state energy surface of azobenzene. A number of linear anilinepyridinium donor-bridge-acceptor chromophores was examined using Q^{VECD} to unravel the influence of its pi-conjugated bridge on charge separation. Finally, the usefulness of the presented method as a tool in optimizing charge transfer is shown for a homologous series of organometallic pigments. The presented work allows facile calculation of a novel, relevant quantity describing charge transfer processes at the atomic level. © 2017 The Authors Journal of Computational Chemistry Published by Wiley Periodicals, Inc.

DOI: 10.1002/jcc.24822

Introduction

Molecular photophysical processes can be described conceptually with a Jablonski diagram and an energy profile that plots surfaces for ground and excited states S_0, S_1, ... (Fig. 1). Hence, experimentally determined energies can be predicted theoretically with time-dependent density functional theory (TD-DFT), thereby enabling *in silico* design of photoactive materials. In the past decade such calculations have been conducted on large molecules (<200 atoms) to explore the effect of light absorption on the reorganization of electron density, which is relevant to the design of light-driven molecular motors[1] and switches,[2] singlet[3a] and triplet[3b] photocatalysts, and light-harvesting architectures.[4]

Electron density difference isosurface plots can be used for the purpose of obtaining an in-depth atomistic view (Fig. 2) of photoexcitation, but such analyses are only qualitative and give no information about the magnitude of the change in density. Moreover, electron density difference isosurfaces are poorly defined when nuclear positions are affected by the photophysical process, which hampers a proper description of the relaxation process.

In this pursuit, Le Bahers, Adamo, and Ciofini[5] pioneered a quantitative analysis that has been useful in the analysis of light-absorbing organic chromophores.[6] In their approach the charge transferred (q^{CT}) in a photochemical transition is calculated from the sum of all per-atom differences in partial atomic charges (PAC) having the same sign. The associated vector d^{CT}, across which charge is transferred, is computed between the geometric barycenters of the positive and negative PAC difference. The difference in electron density is used to compute PACs, but any method of obtaining partial charges can in principle be applied. Jacquemin et al. investigated the relative merits of various PAC schemes to calculate q^{CT}/D^{CT}.[5c] This CT index has been adapted to also include excitation-induced geometrical changes, thereby enhancing its utility in, for example, excited-state proton transfer processes.[7]

Other indices that quantify electron density differences, such as the density overlap index ϕ_s[8a] or the molecular orbitalderived hole-electron difference Δ_r[8b] have been developed as well. These approaches provide global quantitative data on a molecular system. However, from such single (per-molecule) values or indices, no fine-grained information on per-atom charge differences can be obtained.

We felt the need to develop a mathematically straightforward method capable of describing at the atomic level the effect of electronic transitions and relaxations on charge distribution. Atomic charges computed for the initial state of a photochemical process are then subtracted from those at the final state. By subtracting state-specific electron densities for atoms (or groups of atoms) that are numerically integrated over the Voronoi polyhedra, we arrive at a *quantitative* description of charge transfer in vertical excitations and relaxations.

[a] *J. A. Rombouts, A. W. Ehlers, K. Lammertsma*
Department of Chemistry and Pharmaceutical Sciences, Vrije Universiteit Amsterdam, De Boelelaan 1083 & 1085, Amsterdam, HV, +1081 The Netherlands
E-mail: a.w.ehlers@vu.nl and k.lammertsma@vu.nl
[b] *A. W. Ehlers, K. Lammertsma*
Department of Chemistry, University of Johannesburg, Auckland Park, Johannesburg, South Africa 2006
Contract grant sponsor: BioSolar Cells Programme of the Dutch Ministry of Economic Affairs (J.A.R.)

These results appear more robust compared with other space-partitioning (Bader and Hirschfeld) and wavefunction-based partitioning (Mulliken) methods.

Approach

Summing electron density of atom-centered Voronoi cells has been used previously to obtain ground-state electronic charges.[9] We forego the inclusion of a promolecule density in our calculations for reasons of simplicity (Had we employed the VDD by Bickelhaupt et al., the promolecule density would eventually cancel out in the equation $Q = Q^{\text{final}} - Q^{\text{initial}}$).The electron density is computed for each point of interest on the ground and excited state of the potential energy surfaces. The atomic Voronoi charge $Q^{Voronoi}{}_{\text{Atom}}$ for all atoms is defined according to eq. (1), which integrates electron density over atom-centered Voronoi polyhedra, and is expressed in units of charge as fraction of the charge of one electron. The $Q^{Voronoi}$ charges must be computed separately for the initial and final states to determine the $Q^{\text{VECD}}_{\text{Atom}}$ values for each atom in a photochemical step, according to eq. (2). For emission Q^{VECD} the Voronoi charges at the excited state S_1^E must then be subtracted from the ground state charges S_0^E, both calculated at the excited state geometry (denoted by superscript E). It is important to recognize that there does not exist a unique set of Voronoi polyhedra if the atomic coordinates change between initial and final state. In these cases, direct integration of the density difference $\Delta\rho(r)$ in eq. (1) would be an undefined operation, making obvious the use of eq. (2). Finally, for a group of atoms R, the summed Voronoi charge $Q^{\text{VECD}}_{\text{R}}$ is defined by eq. (3).

$$Q^{\text{Voronoi}}_{\text{Atom}} = \int_{\substack{\text{Voronoi polyhedron}\\ \text{of the atom}}} \rho(r)dr \quad (1)$$

$$Q^{\text{VECD}}_{\text{Atom}} = Q^{\text{Voronoi}}_{\text{Atom, final}} - Q^{\text{Voronoi}}_{\text{Atom, initial}} \quad (2)$$

$$Q^{\text{VECD}}_{\text{R}} = \sum_{\substack{\text{all atoms}\\ \text{A in R}}} Q^{\text{VECD}}_{\text{Atom}} \quad (3)$$

Method validation

Other methods to calculate PAC, such as Bader,[10] Hirschfeld,[11] and Mulliken[12] charge analyses are also readily obtained with DFT software packages. For arbitrary PAC frameworks, a straightforward extension to excitation charge difference is to subtract the excited state charge for each atom A from that of its ground state. For example, we define Bader excitation charge differences (BECD) as in eq. (4). Other quantities such as $Q^{\text{VECD}}_{\text{A}}$ are defined in an analogous manner.

$$Q^{\text{BECD}}_{\text{A}} = Q^{\text{Bader}}_{\text{A, final}} - Q^{\text{Bader}}_{\text{A, initial}} \quad (4)$$

The Bader (BECD), Hirschfeld (HECD), Mulliken (MECD), and Voronoi (VECD) charge differences were compared for vertical transitions of diatomic and other small molecules with varying dipole moments using Dunnings' correlation-consistent polarized basis sets of double, triple, quadruple and quintuple zeta quality, with and without diffuse functions, i.e., cc-pVDZ, cc-pVTZ, cc-pVQZ, cc-pV5Z, aug-cc-pVDZ, aug-cc-pVTZ, aug-cc-pVQZ, and aug-cc-pV5Z).

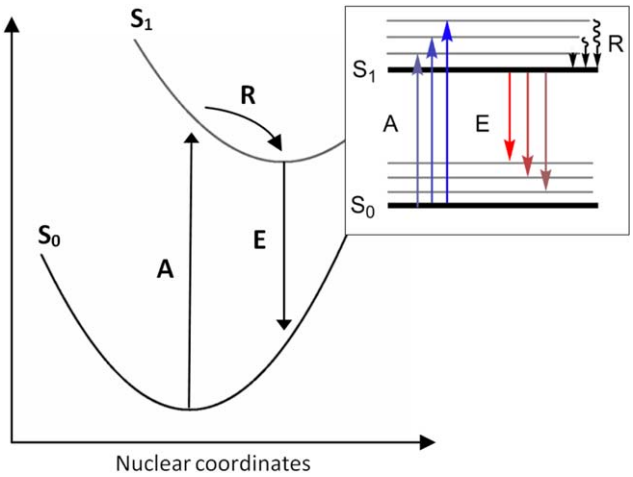

Figure 1. Jablonski diagram (top right) showing excitation A from the ground state into allowed vibrational levels of the first singlet excited state S_1. Internal relaxation R followed by emission E returns the compound to any of the allowed vibrational ground state modes. The energy profile (left) foregoes the description of vibrational fine structure by simply describing absorption and emission as vertical transitions from energy minima into off-equilibrium geometries on another potential energy surface. [Color figure can be viewed at wileyonlinelibrary.com]

The results for the n $\rightarrow$ π^* excitation of formaldehyde are plotted in Figure 4, showing computed charge as a function of basis set. The Q_O/Q_C ratio is expected to be near unity, because the hydrogen atoms do not participate in the pi-bond affected by this excitation (see also the left panel of Fig. 2). The Mulliken Q_O/Q_C charge ratios are highly dependent on the basis set in accordance with prior observations.[9] The Bader-derived values predict an accumulation of charge on carbon, with Q_O/Q_C ratios fluctuating between 50% and 60%. The Hirschfeld ratios perform better and show a convergence

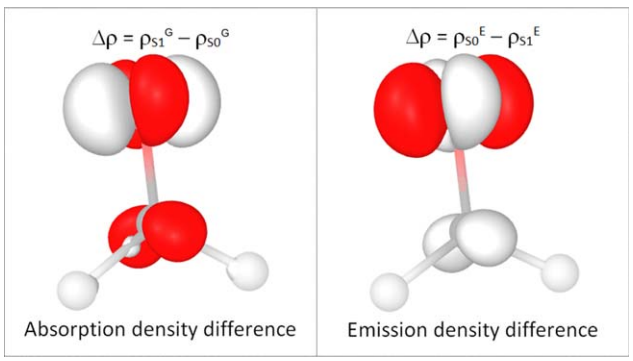

Figure 2. Charge density difference plot of the n $\rightarrow$ π^* absorption in formaldehyde. Surfaces describe the electron density differences $\Delta\rho$ for absorption and emission at a fixed isocontour value of 0.025, calculated by subtracting the final electron density from the initial one. Absorption means depletion (white shaded lobes) of the non-bonding oxygen centered MO and accumulation of charge in the anti-bonding π^* MO. Conversely, depletion of the non-bonding π^* is observed for emission. Volumes shaded in red are depleted of electron density on going from the initial to the final state. [Color figure can be viewed at wileyonlinelibrary.com]

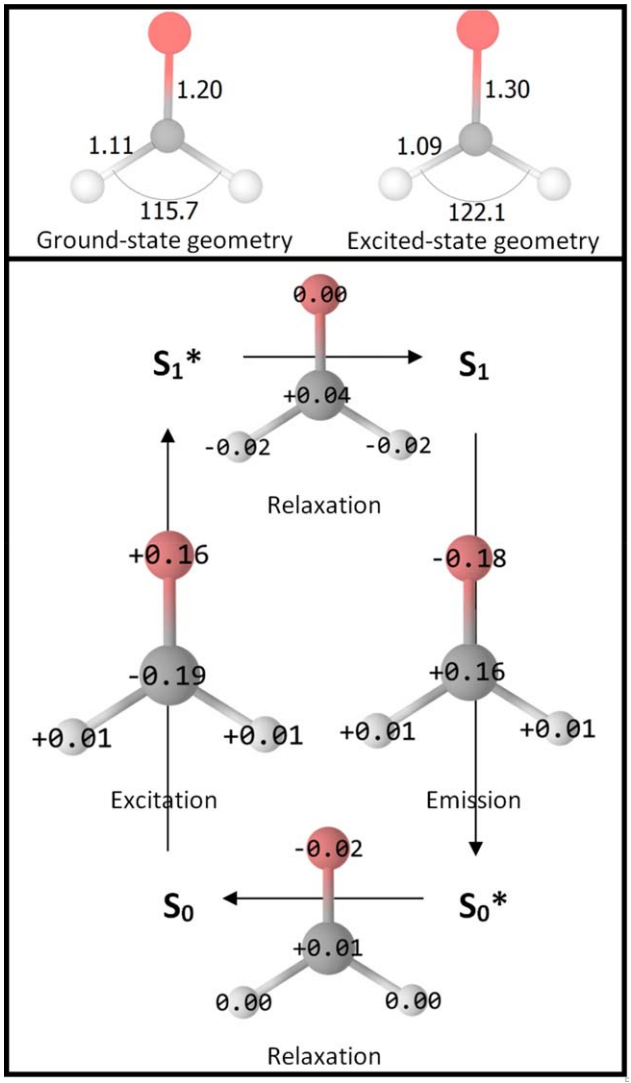

Figure 3. Ground- and excited-state geometries of formaldehyde at B3LYP/aug-cc-pVTZ (top) with atomic Q^{VECD} charges (bottom) for the n $\rightarrow$ π^* excitation-emission cycle. A negative value denotes the rearrangement of electron density toward the nucleus. The non-zero sum of charges are due to rounding errors, see Supporting Information. [Color figure can be viewed at wileyonlinelibrary.com]

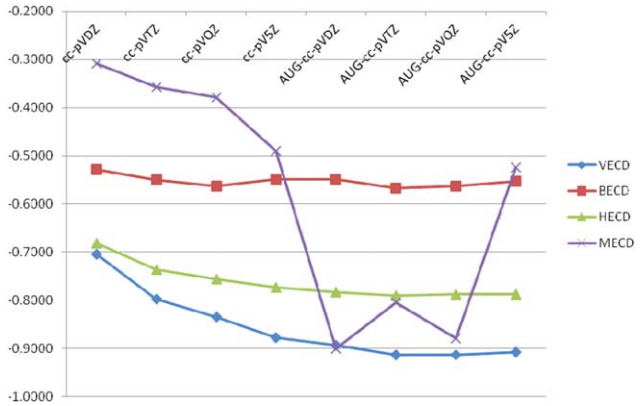

Figure 4. Plot of the ratio between accumulated charge on oxygen and carbon as a function of basis set, computed using a subtraction of Voronoi, Bader, Hirschfeld, and Mulliken charges for n $\rightarrow$ π^* excitation of formaldehyde. [Color figure can be viewed at wileyonlinelibrary.com]

to nearly 80%, but the Voronoi Q_O/Q_C ratio goes beyond 90% even though its partitioning is arguably the most simple one. The slightly inferior ratio obtained using Hirshfeld may be due to the 'sharing factor'[11] that 'smoothes' partial charges across neighboring atoms.

The basis set dependency on the entire set of test molecules can be quantified using the standard deviation across all basis sets (σ_A) for all atoms (A). The sum $\Sigma\sigma_A$ reflects the performance with higher values indicating poorer consistency between basis sets (e.g., for nitrous oxide $\Sigma\sigma(NNO) = \sigma(N_1) + \sigma(N_2) + \sigma(O)$ where $\sigma(N_1)$, $\sigma(N_2)$, ... is the standard deviation of Q^{VECD} over all the used basis sets, for an atom). Figure 5 displays the performance of PACs across the molecules in the test set; a comprehensive table is given in the Supporting Information. Again, the Voronoi charge difference analysis outperforms that of the Hirshfeld analysis. The results are worse on using the Bader approach, with higher basis set dependence for all compounds in the test set. The large standard deviation in this case is possibly due to use of zero-flux surfaces as a basis for spatial partitioning, since these are inherently dependent on the chosen electronic state (Bader analysis has to compute, for every given electron density, the Bader surfaces that partition space into atomic volumes. For Voronoi, every set of Cartesian coordinates has one and only one partitioning that is independent on electron density). Mulliken charges are highly variable and are clearly unsuited for performing the desired charge difference calculations. Due to its superior performance Voronoi-based charge differences are used in the rest of this study.

It is relevant to address the practical aspects of calculating the Q^{VECD} values. Most quantum chemical software packages give electron densities as voxel files in which a series of volume elements (voxels) describe the density around the molecule. Assignment of subtracted charge density to the nearest neighboring atom is straightforward and entails computing the nearest atom to the position of the current voxel, subtracting the two charge densities, accumulating the resulting number on the nearest nucleus, and advancing one position. A script written in the Python language that performs these

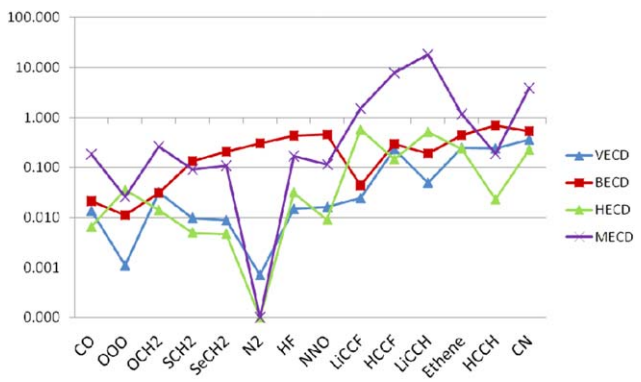

Figure 5. Effect of various schemes for computing PAC on $\sum\sigma_A$ for 14 test molecules, plotted on a logarithmic scale. Larger values indicate a higher basis set dependence. [Color figure can be viewed at wileyonlinelibrary.com]

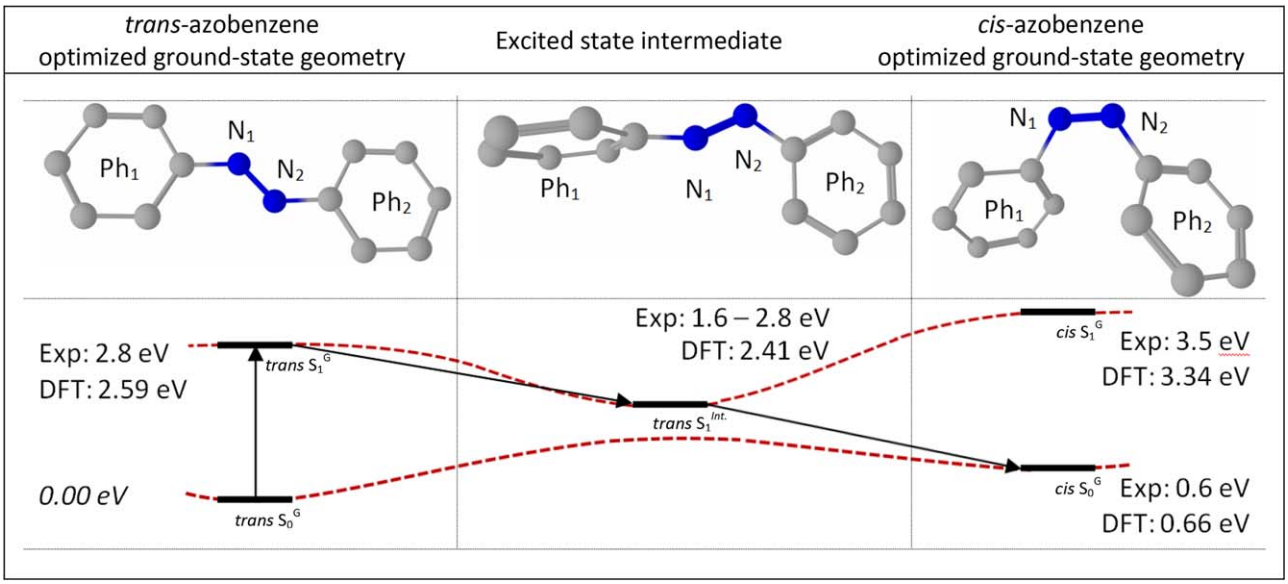

Figure 6. Energy diagram for the excitation–relaxation–nonradiative decay process for *trans*-azobenzene isomerization to *cis*-azobenzene (black arrows). Experimental energies taken from literature.[13] Both experimental and (TD)-DFT derived energies are translated to correspond to 0.00 eV at *trans*-azobenzene, the lowest energy state. The captions shown correspond to the groups of atoms used to tabulate results in Table 1. Dotted red lines indicate the shape of the potential energy surfaces. [Color figure can be viewed at wileyonlinelibrary.com]

calculations on the popular cube files (as generated by, e.g., ADF, NWChem, and Gaussian) is available in the Supporting Information.

Voronoi Charge Difference Analysis for Formaldehyde $\pi - \pi^*$ Excitation

We start with formaldehyde and examine the excitation from its non-bonding lone pair centered on oxygen to the π^* orbital. A four-step cycle describes the photon absorption, geometry relaxation of the excited molecule, photon emission, and geometrical relaxation on the ground state surface (Fig. 3). For each of these steps the change in charge distribution on every atom was calculated with eqs. (1) and (2).

The computed atomic Q^{VECD} values concur with the isocontour map of Figure 2, as charge is removed from the oxygen atom-centered lone pair on excitation and returned on emission; the influence from the hydrogen atoms is small because they do not contribute to the π^* orbital. A small but relevant charge difference is observed on relaxation of both the exited ($S_1^* \rightarrow S_1$) and ground-state ($S_0^* \rightarrow S_0$) structures. Clearly, compared to density isocontour plots, the Voronoi Charge Difference method gives a comprehensive analysis of the entire photochemical cycle.

Relaxation-Induced Charge Transfer in *Trans*-Azobenzene

In contrast to the limited nuclear motion possible in the small and rigid formadelhyde molecule, more significant relaxation-associated nuclear motions are expected when studying compounds with a larger number of degrees of freedom. Such a well-studied chromophore is azobenzene, which famously undergoes reversible photoisomerization from the more stable *trans* conformer to the *cis* conformer.[13] Its rich excited state photochemistry has been the cornerstone of molecular designs such as light-driven molecular motors, photochemically controlled molecular switches or design into light-responsive functional materials.[14] Thus, it is of interest to probe the Q^{VECD} values on the process from photoexcited *trans*-azobenzene, through an intermediate excited-state geometry, to *cis*-azobenzene.

The photochemical process under study is based on the assumption that *trans* – *cis* isomerization occurs by means of vertical excitation from the ground-state *trans* geometry to S_1, followed by relaxation on the S_1 energy surface to an intermediate excited-state geometry, and finally nonradiative decay to the *cis*-azobenzene ground state geometry.

We have based this pathway, shown in Figure 6, on spectroscopic investigations that conclude that isomerization takes place from the S_1 energy surface.[15] As such, probing electron density rearrangement during azobenzene isomerization should initially target the vertical excitation from ground state to S_1.

Second, for azobenzene, there are no well-defined energy minimums on S_1 to which the excited compound can be said to relax, as the S_1 – S_0 surfaces have been shown to contain crossing seams and conical intersections[16] via which nonradiative relaxation proceeds directly to ground state *cis*-azobenzene. Due to these complications, a thorough computational treatment of the isomerization process is beyond the scope of this work. We define an excited state geometry that is intermediate between the two ground state structures by applying some torsion to one of the C-C-N-N dihedral angles (see Fig. 6, top), with the caveat that other intermediate geometries can and probably do exist. This structure is optimized in the S_1 excited state using TD-DFT to suitable convergence of energy, density and gradient. Experimental work by Satzger et al.[13]

Table 1. Computed Q^{VECD} values of each step in the above isomerization process, for the separate nitrogen atoms and summed over each phenyl group, as described for the latter in eq. (3).

Process step description	Ph_1	Ph_2	N_1	N_2
trans S_0^G to *trans* $S_1^{G[a]}$	−0.058	−0.058	+0.059	+0.058
trans S_0^G to $S_1^{Int.[b]}$	+0.206	−0.129	−0.019	−0.059
$S_1^{Int.}$ to *cis* $S_0^{G[c]}$	−0.104	+0.250	−0.098	−0.048
Overall *trans* to *cis*	+0.044	+0.063	−0.058	−0.048
cis S_0^G to *cis* $S_1^{G[d]}$	+0.016	+0.016	−0.016	−0.016
cis S_0^G to $S_1^{Int.[d]}$	+0.088	−0.266	+0.144	+0.064
$S_1^{Int.}$ to *trans* $S_0^{G[d]}$	−0.148	+0.187	−0.040	−0.000
Overall *cis* to *trans*	−0.044	−0.063	+0.058	+0.048

[a] Vertical excitation from *trans*-azobenzene. [b] Relaxation to $S_1^{Int.}$, the excited state intermediate structure as defined in the text. [c] Non-radiative decay to the *cis*-azobenzene ground state. [d] Process steps for the back-reaction from *cis*-azobenzene to *trans*-azobenzene, via an identical excitation–relaxation–decay pathway. Negative values signify net accumulation of electrons

serves to validate our computed energies, also showing that the energy of the intermediate conforms to spectroscopic data. Finally, Voronoi charge difference from this excited state geometry toward the *cis*-azobenzene ground state is computed.

Shown in Table 1 are computed Q^{VECD} values for both nitrogen atoms and summed values for each phenyl ring in the azobenzene isomers. The table shows computed values for the forward *trans* to *cis* reaction as well as the reverse isomerisation via an identical excitation – relaxation – decay pathway. For the vertical $S_0 \rightarrow S_1$ transition, there is less computed charge transfer for absorption and emission compared to the strongly polarized C = O bond in formaldehyde. This can be explained by the localization of both HOMO and LUMO orbitals around the N = N bond. A large effect on charge distribution on photoisomerization can be observed for the relaxation and decay steps. The broken C_{2h} symmetry of the intermediate geometry is reflected in the preferential location of electrons on one of the phenyl rings during relaxation ($Q_{Ph1}^{VECD} = +0.206$ e, $Q_{Ph2}^{VECD} = -0.129$ e); negative charge accumulates at the phenyl ring labeled Ph2 which remains conjugated to the azo bond. The electrons move in the opposite direction during the final step toward the *cis* geometry ($Q_{Ph1}^{VECD} = -0.104$ e, $Q_{Ph2}^{VECD} = +0.250$ e). Eventually this leads to a net difference in charge distribution after isomerisation to *cis*-azobenzene: a total Q^{VECD} charge of + 0.106 is removed from the nitrogen atoms and moved to the phenyl groups (overall Q_{N1}^{VECD} + overall $Q_{N2}^{VECD} = +0.106$ e; Table 1).

Clearly, Q^{VECD} calculations are able to elucidate charge transfer associated with light-driven geometry changes in this compelling compound and should assist the physical organic chemist in designing matter that combines light-driven molecular motion with charge transfer properties. For example, these calculations could allow *a priori* prediction of the effect of chemical substitution of the phenyl rings with various sterically demanding groups, forcing the selective accumulation of charge on one end of the compound, thereby potentially producing molecular diodes.[17]

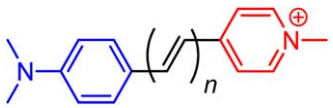

Figure 7. Color-coded partitioning scheme used for the summed Q^{VECD} charges. The *p*-dimethylaminophenyl (blue) group is the donor, the olefin (black) is the bridge, and the methylpyridinium (red) fragment is the acceptor. [Color figure can be viewed at wileyonlinelibrary.com]

Long Range Charge Transfer in a Donor-Bridge-Acceptor Dye

To quantify the influence of the distance between donor and acceptor on charge transfer in photoactive chromophores, we examine in this section the applicability of Q^{VECD} calculations to increasingly larger linear donor-acceptor dyes and test the conformity of our results to what is expected for such molecules. *trans*-4-[4-(Dimethylamino)styryl]-N-methylpyridinium iodide (DAMPI, Fig. 7) is a versatile light-absorbing dye used in non-linear optics,[18] spectroscopy,[19] and zeolite morphology research.[20] Two absorption maxima are observed in organic solvents, one around 500 nm and one upwards of 300 nm.[21] The molecular structure suggests push-pull behavior in which electrons move from the aniline moiety to its electron-poor pyridinium group.[22] Fluorescent emission (aqueous solvents) shows a redshift from 470 to 600 nm,[23] suggesting excited-state relaxation behavior.

The cam-B3LYP/cc-pVTZ (COSMO) optimized ground and excited state structures of DAMPI (in DCM) were analyzed by single point TDDFT calculations for the vertical $S_0 \rightarrow S_1$ excitation (corresponding to a push-pull, HOMO → LUMO, $\pi \rightarrow \pi^*$ transition), relaxation, and emission. A long-range hybrid functional was used to accommodate the excited-state properties of the push-pull chromophore.[24] The Q^{VECD} values are summed into 'donor', 'bridge', and 'acceptor' parts (see color coding in Fig. 7) according to eq. (3), listed in Table 2, and displayed in Figure 8.

The parent DAMPI ($n = 1$) is indeed a charge transfer chromophore with negative charge being moved from the dimethylaniline donor to the N-methylpyridinium acceptor on excitation. The bridge accumulates only 10% of charge on the two olefinic carbons. Subsequent relaxation enhances the charge transfer significantly due to additional polarization of the donor and acceptor sites. The graphical presentation of the Q^{VECD} values for the photochemical cycle in Figure 8 illustrates that relaxation of the excited state maximizes the polarization, which largely reverses on emission and disappears on subsequent relaxation, as it should.

Table 2. Q^{VECD} values for the dimethylaniline donor, ethylene bridge, and N-methylpyridine acceptor groups of atoms.

	Donor	Bridge	Acceptor
Excitation	+0.191	−0.022	−0.169
S1 relaxation	+0.063	−0.009	−0.057
Emission	−0.373	+0.046	+0.326
S0 relaxation	+0.188	−0.019	−0.100

Values are computed for excitation, excited state relaxation, emission, and ground-state relaxation steps. Negative values signify accumulation of electrons.

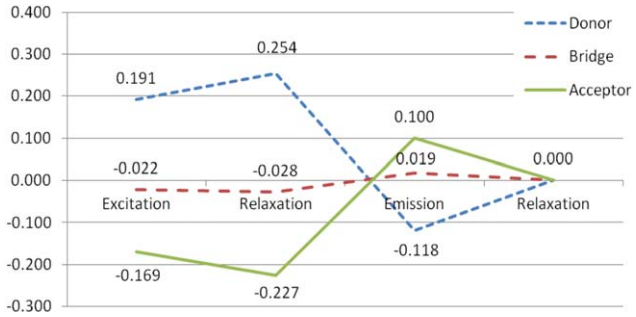

Figure 8. Q^{VECD} charges on DAMPI donor, bridge, and acceptor groups, for the four steps of the photochemical cycle. Positive values signify net charge depletion and negative ones net accumulation of electrons. [Color figure can be viewed at wileyonlinelibrary.com]

Next, the influence of differently sized bridges ($n = 0$, 1, 2, 3 in Fig. 7) was evaluated for the vertical excitation induced charge transfer from the dimethylaminophenyl donor to the methylpyridine acceptor using cam-B3LYP/cc-pVTZ. To assess the charge transfer efficiency of the DAMPI homologues, we computed the charge transfer vectors D^{CT} according to Ciofini et al.[5] The results show that for every 2.5 Å added to the length of the compound, which is the size of a repeating ethylene unit, the charge transfer distance increases by only ~0.3 Å. This observation concurs with earlier studies on linear donor-acceptor systems[25] where it was found that elongation can decrease the donor-to-acceptor charge transfer efficiency. The Q^{VECD} values for these DAMPI homologues, listed in Table 3, show a decrease in charge transfer on elongation of the olefinic bridge. The transferred charge decreases by 60% on going from $n = 0$ to $n = 3$. We attribute this behavior to increased Coulomb interaction concomitant with the increase in donor-acceptor distance, causing the oligoethylene spacer to become involved in charge transfer as shown for similar linear donor-bridge-acceptor systems.[25] From the Q^{VECD} calculations valuable numerical insights are gained into the magnitude of charge accumulated across the ends of the homologues.

Electron Transfer in Chromophoric Metallosalphen Compounds

Finally, in this section we explore Q^{VECD} as a design tool for the preparation of organometallic pigments. Recently, we reported on the synthesis of DATZnS (Fig. 9) as building block for supramolecular light-harvesting architectures.[26] This flat molecule that contains a conjugated naphthalene diimide

Table 3. Q^{VECD} values and charge transfer vectors D^{CT} (see text, via Ciofini et al.[17]) for vertical excitation of the donor, bridge, and acceptor moieties of DAMPI analogues.

	Donor Q_R^{VECD}	Bridge Q_R^{VECD}	Acceptor Q_R^{VECD}	D^{CT}
$n = 0$	+0.239	*N.A.*	−0.241	2.50 Å
$n = 1$	+0.191	−0.022	−0.169	2.71 Å
$n = 2$	+0.164	−0.017	−0.148	3.09 Å
$n = 3$	+0.139	−0.022	−0.121	3.39 Å

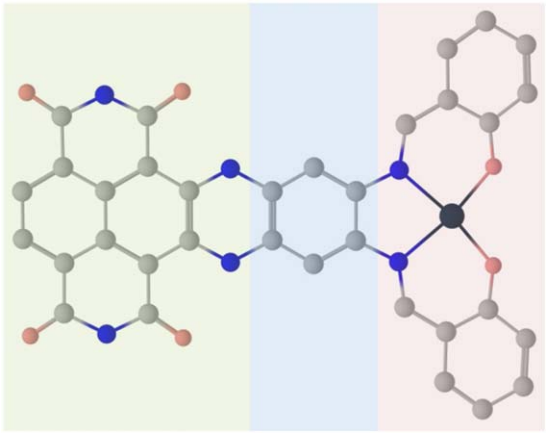

Figure 9. Molecular structure of DATMS. The shaded areas indicate the grouping of Q^{VECD} charges according to eq. (3). The naphthalene diimide is at the left (green), the bridging phenylene in the middle (blue), and the salphen ligand arms (red) on the right, chelating a metal cation (M; black). Red atoms = oxygen, gray = carbon, blue = nitrogen, black = metal; hydrogen atoms are omitted for clarity. [Color figure can be viewed at wileyonlinelibrary.com]

fused to a Zn^{II}-binding tetradentate 'salphen' moiety was shown to emit from a singlet excited state on photoexcitation. Supramolecular binding of a fifth ligand to the zinc cation appears to have no effect on the photophysical properties of DATZnS,[26b] leading to the conclusion that the metal site serves a purely structural purpose. Replacing the inert d^{10} Zn^{II} cation for other d-block metals of different redox activity may, however, affect the chromophoric properties. We investigate the effect of different metals on the absorption properties using Q^{VECD} calculations.

To this end, we examined the first-row d-block Ni^{II}, Fe^{II}, Cu^{I}, Co^{I}, and Co^{III} analogues, having the generic abbreviation DATMS. Their choice was based on the synthetic accessibility of the parent salphen complexes[27] and their $S = 0$ spin state, which also simplifies the TDDFT calculations (see Supporting Information for details). We investigated for each compound the first singlet excitation with non-zero oscillator strength. Table 4 shows the TDDFT-derived orbital configurations of the singlet excitations under study.

Table 4 lists the computed Q^{VECD} charges for the DATMS series as sums of the atomic charge differences (eq. (3)) found on the naphthalene diimide (NDI), phenylene bridge, salphen ligand arms and metal atom (see Fig. 9). They allow for an evaluation of the degree and direction of the charge transfer in the chromophore with respect to the electropositive character of the d-block metal. The three neutral analogues with a formally dicationic metal (Fe^{II}, Ni^{II}, and Zn^{II}) have virtually identical properties. The Q^{VECD} charges are accumulated in the NDI unit, ranging from −0.118 to −0.111, and originate in equal degrees from the salphen and phenylene bridge. Clearly, moving from a d^{10} configuration (Zn^{II}) to a low-spin d^6 (Fe^{II}) has little influence on the magnitude of charge transfer, the absorption wavelength, and the orbital configuration of the optical transition. This indicates that the charge transfer behavior for the neutral compounds is determined by the properties of the organic ligand and not by the metal.

Table 4. Q^{VECD} values for the first vertical optical transition with non-zero (> 0.01) oscillator strength in various first-row analogues of DATZnS.

Compound name[a]	Co(III) $DATCoS^{+1}$	Co(I) $DATCoS^{-1}$	Cu(I) $DATCuS^{-1}$	Fe(II) DATFeS	Ni(II) DATNiS	Zn(II) DATZnS
Q^{VECD} on NDI[b,c]	+0.125	−0.001	−0.265	−0.111	−0.116	−0.118
Q^{VECD} on bridge[b,c]	+0.015	−0.021	+0.040	+0.049	+0.052	+0.054
Q^{VECD} on ligand[b,c]	−0.088	−0.091	+0.219	+0.063	+0.062	+0.060
Q^{VECD} on metal[b,c]	−0.051	+0.112	+0.006	−0.001	+0.002	+0.005
TDDFT energy	1.87 eV	1.53 eV	2.14 eV	2.59 eV	2.59 eV	2.57 eV
Oscillator strength	0.20	0.12	1.21	1.45	1.48	1.46
Donor MO[d]	HOMO-2	HOMO	HOMO-1	HOMO	HOMO	HOMO
Acceptor MO[d]	LUMO	LUMO+1	LUMO	LUMO	LUMO	LUMO

[a] Superscripts in the compound names denote non-zero overall charge where applicable. [b] The Q^{VECD} charges are summed into the groups of atoms shown in Figure 9. [c] See Figure 9 for the atomic groupings used. [d] The configuration of the donor and acceptor MO's most strongly (>75% contribution) associated with the calculated transition is shown.

A different picture emerges for the charged analogues. Comparing the d^{10} anionic $DATCuS^{-1}$ to DATZnS shows an approximate threefold increase of charge depletion on the salphen ligands ($Q^{VECD} = +0.219$), and a twofold increase of charge transfer to the electron-accepting NDI moiety ($Q^{VECD} = -0.265$). The electron transfer for this Cu^{I} congener results from excitation from the ligand-based HOMO-1 to the LUMO, which is located at the NDI (similar to DATZnS, see isocontour plots in Fig. 10), showing $DATCuS^{-1}$ as an improved version of the original Zn-containing chromophore.

In contrast, $d^{[8]}$ anionic $DATCoS^{-1}$ shows negligible charge transfer to the NDI on photoexcitation. Instead, charge is transferred to the salphen ligands ($Q^{VECD} = -0.091$) and removed from the metal atom ($Q^{VECD} = +0.112$). As the MLCT state does not extend appreciably past the salphen arms it appears that the more electropositive Co^{I} is not capable (like Cu^{I}) of donating to the NDI's LUMO. Here, numerical analysis using Q^{VECD} allows to precisely pinpoint the results of substituting the parent compound with a less electronegative metal.

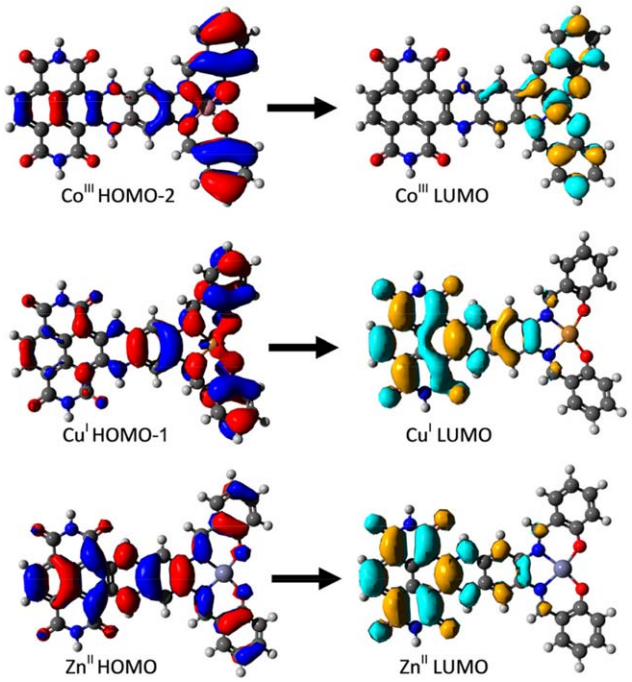

Figure 10. Molecular orbital surfaces for $DATCoS^{+1}$, $DATCuS^{-1}$, and DATZnS (top to bottom) plotted at an isocontour value of 0.02. [Color figure can be viewed at wileyonlinelibrary.com]

Remarkably, cationic d^6 compound $DATCoS^{+1}$ shows a complete reversal of the photodriven charge transfer, namely from the NDI ($Q^{VECD} = +0.125$) to the salphen ($Q^{VECD} = -0.140$; see also Fig. 10). The ligand-to-metal charge transfer concurs with the expected behavior for electropositive metals. This umpolung of the NDI redox chemistry, where the usually electron-demanding NDI is changed from a reductor to an oxidant, is in line with literature reports that show the use of an NDI as cation sensor capable of undergoing one-electron reduction.[28]

The directionality of charge transfer is clear: the electron-rich metal complexes transfer charge away from the metal, whilst the electron poor Co^{III} complex transfers charge toward the metal. Using Voronoi charge differences, these qualitative descriptions can be assigned a numerical quantity, which will clearly be of benefit to exploratory and explanatory molecular research.

Conclusions

The presented method that makes use of atom-centered Voronoi polyhedra to calculate charge differences for photoinduced excitations and emissions provides an easily obtainable, novel, and relevant quantity to describe charge transfer processes at the atomic level. Because electron charge is integrated over atomic volumes before subtracting the initial state properties from the final state properties, both vertical processes and those that incur geometrical changes can be assessed using the Q^{VECD} formalism.

There is a direct correspondence of Q^{VECD} values with the well-known, intuitive but strictly qualitative electron density isocontour plots, as showcased for formaldehyde. For a series of donor-bridge-acceptor chromophores, Q^{VECD} values are shown to be consistent with existing methods of assessing photodriven charge transfer. Computation of the Voronoi excitation charge difference can be employed as a design tool to optimize charge transfer processes, as shown for a series of chromophoric metal complexes. By quantifying the amount of

charge moving across the donor-acceptor axis of the molecule, direct comparison across a homologous series of compounds is possible. We believe this to be an excellent example of the value of Q^{VECD} calculations as a design tool for photoactive organic compounds. Furthermore, the calculations add quantitative insight to the qualitative description available through MO theory.

The chosen Voronoi partitioning scheme is density-independent, that is, the obtained atomic volumes depend only on atomic coordinates and not on the DFT-derived electron density. As such, this method is expected to be equally applicable to processes in singlet, triplet or open-shell systems, which is a topic for future study.

In reflecting on the Bader versus Voronoi approach, we note that Tognetti and Joubert et al.[29] have shown that charge transfer vector (D^{CT} and q^{CT}) calculations based on integration over Bader volumes are much improved on taking into account the positive atomic charge Z. For our Q^{VECD} calculations on vertical processes, Z would simply vanish from the equation, but changes in geometry cause changes in integrated volumes. Hence, the role of atomic dipoles in Q^{VECD} calculations on processes with changing nuclear positions is an intriguing topic for further study.

Acknowledgments

Matus Telgarsky is acknowledged for helpful discussions on implementing the Q^{VECD} algorithm in a Python script and Frank Hendriks for suggesting the use of the DAMPI scaffold.

Keywords: time-dependent density functional theory · atomic charges · charge analysis · molecular design

How to cite this article: J. A. Rombouts, A. W. Ehlers, K. Lammertsma. *J. Comput. Chem.* **2017**, *38*, 1811–1818. DOI: 10.1002/jcc.24822

Additional Supporting Information may be found in the online version of this article.

[1] B. L. Feringa, N. Koumura, R. W. J. Zijlstra, R. A. Van Delden, N. Harada, *Nature* **1999**, *401*, 152.
[2] W. Yang, Y. Li, H. Liu, L. Chi, Y. Li, *Small* **2012**, *8*, 504.
[3] (a) L. Wu, B. Chen, Z. Li, C. Tung, Acc. Chem. Res. **2014**, *47*, 2177; (b) J. Zhao, W. Wu, J. Sun, S. Guo, *Chem. Soc. Rev.* **2013**, *42*, 5323.
[4] P. D. Frischmann, K. Mahata, F. Wurthner, *Chem. Soc. Rev.* **2013**, *42*, 1847.
[5] (a) T. Le Bahers, C. Adamo, I. Ciofini, J. Chem. Theory Comput. **2011**, *7*, 2498; (b) G. Garcia, C. Adamo, I. Ciofini, *Phys. Chem. Chem. Phys.* **2013**, *15*, 20210; (c) D. Jacquemin, T. Le Bahers, C. Adamo, I. Ciofini, *Phys. Chem. Chem. Phys.* **2012**, *14*, 5383.
[6] A. M. Grabarz, B. Jędrzejewska, A. Zakrzewska, R. Zaleśny, A. D. Laurent, D. Jacquemin, B. Ośmiałowski, *J. Org. Chem.* **2017**, *82*, 1529.
[7] C. Adamo, T. Le Bahers, M. Savarese, L. Wilbraham, G. García, R. Fukuda, M. Ehara, N. Rega, I. Ciofini, *Coord. Chem. Rev.* **2015**, *304*, 166.
[8] (a) T. Etienne, X. Assfeld, A. Monari **2014**, *10*, 3896; (b) C. A. Guido, P. Cortona, B. Mennucci, C. Adamo **2013**, *9*, 3118.
[9] C. F. Guerra, J. Handgraaf, E. J. Baerends, F. M. Bickelhaupt, *J. Comput. Chem.* **2004**, *25*, 189.
[10] R. F. W. Bader, P. M. Beddall, *J. Chem. Phys.* **1972**, *56*, 3320.
[11] F. L. Hirshfeld, *Theor. Chim. Acta* **1977**, *44*, 129.
[12] R. S. Mulliken, *J. Chem. Phys.* **1955**, *23*, 1833.
[13] H. Satzger, S. Sporlein, C. Root, J. Wachtveitl, W. Zinth, P. Gilch, *Chem. Phys. Lett.* **2003**, *372*, 216.
[14] (a) A. Credi, Aust. J. Chem., **2006**, *59*, 157; (b) M. Saccone, V. Dichiarante, A. Forni, A. Goulet-Hanssens, G. Cavallo, J. Vapaavuori, G. Terraneo, C. J. Barrett, G. Resnati, P. Metrangolo, A. Priimagi, *J. Mater. Chem. C*, **2015**, *3*, 759; (c) O. Nachtigall, C. Kordel, L. H. Urner, R. Haag, *Angew. Chem. Int. Ed.* **2014**, *36*, 9669; (d) A. Cnossen, L. Hou, M. M. Pollard, P. V. Wesenhagen, W. R. Browne, B. L. Feringa, *J. Am. Chem. Soc.* **2012**, *42*, 17613.
[15] T. Fujino, S. Y. Arzjamtsev, T. Tahara, *J. Phys. Chem. A* **2001**, *105*, 8123.
[16] I. Conti, M. Garavelli, G. Orlandi, *J. Am. Chem. Soc.* **2008**, *130*, 5216.
[17] M. del Valle, R. Gutiérrez, C. Tejedor, G. Cuniberti, *Nat. Nanotechnol.* **2007**, *2*, 176.
[18] Y. Mineno, T. Matsukawa, S. Ikeda, T. Taniuchi, H. Nakanishi, S. Okada, H. Adachi, M. Yoshimura, Y. Mori, T. Sasaki, *Mol. Cryst. Liq. Cryst.* **2007**, *463*, 55.
[19] T. Bevilaqua, T. F. Gocalves, C. de G. Venturini, V. G. Machado, *J. Spectrochim. Acta A* **2006**, *65*, 535.
[20] M. B. J. Roeffaers, R. Ameloot, M. Baruah, H. Uji-i, M. Bulut, G. de Cremer, U. Muller, P. A. Jacobs, J. Hofkens, B. F. Sels, D. E. de Vos, *J. Am. Chem. Soc.* **2008**, *130*, 5763.
[21] J. Jeong, J. Kim, J. Campo, S. Lee, W. Jeon, W. Wenseleers, M. Jazbinsek, H. Yun, O. Kwon, *Dyes Pigm.* **2015**, *113*, 8.
[22] P. Kim, J. Jeong, M. Jazbinsek, S. Kwon, H. Yun, J. Kim, Y. S. Lee, I. Baek, F. Rotermund, P. Gunther, O. Kwon, *CrystEngComm* **2011**, *13*, 444.
[23] B. Wandelt, A. Mielniczak, P. Turkewitsch, G. D. Darling, B. R. Stranix, *Biosens. Bioelectron.* **2003**, *18*, 465.
[24] C. Adamo, D. Jacquemin, *Chem. Soc. Rev.* **2013**, *42*, 845.
[25] I. Ciofini, L. Le Bahers, C. Adamo, F. Odobel, D. Jacquemin, *J. Phys. Chem. C* **2012**, *116*, 11946.
[26] (a) B. van den Bosch, J. A. Rombouts, R. V. A. Orru, J. N. H. Reek, R. J. Detz, *ChemCatChem* **2016**, *7*, 1392; (b) J. A. Rombouts, J. Ravensbergen, R. N. Frese, J. T. M. Kennis, A. W. Ehlers, J. C. Slootweg, E. Ruijter, K. Lammertsma, R. V. A. Orru, *Chem. Eur. J* **2014**, *20*, 10285.
[27] (a) A. V. Wiznycia, J. Desper, C. J. Levy, *Chem. Commun.* **2005**, 4693 ; (b) R. Klement, F. Stock, H. Elias, H. Paulus, P. Pelikan, M. Valko, M. Mazur, *Polyhedron* **1999**, *18*, 3617.
[28] M. R. Ajayakumar, D. A. P. Mukhopadhyay, *Org. Lett.* **2012**, *14*, 4822.
[29] (a) V. Tognetti, L. Joubert, *Chem. Phys. Lett.* **2013**, *557*, 150; (b) V. Tognetti, L. Joubert, *Theor. Chem. Acc.* **2016**, *5*, 124.

Received: 23 January 2017
Revised: 12 April 2017
Accepted: 12 April 2017
Published online on 26 May 2017